THE FASEB JOURNAL • RESEARCH • www.fasebj.org

Localization of group II and III metabotropic glutamate receptors at pre- and postsynaptic sites of inner hair cell ribbon synapses

Lisa Klotz,* Olaf Wendler,† Renato Frischknecht,‡ Ryuichi Shigemoto,§ Holger Schulze,¶ and Ralf Enz*,[1]

*Institute for Biochemistry (Emil-Fischer-Zentrum), †Division of Phoniatrics and Pediatric Audiology, Department of Otorhinolaryngology, Head and Neck Surgery, ‡Department of Biology, Animal Physiology, and ¶Department of Otorhinolaryngology, Head and Neck Surgery, Experimental Otolaryngology, Friedrich-Alexander University Erlangen-Nürnberg, Erlangen, Germany; and §Institute of Science and Technology Austria, Klosterneuburg, Austria

ABSTRACT: Glutamate is the major excitatory neurotransmitter in the CNS binding to a variety of glutamate receptors. Metabotropic glutamate receptors (mGluR1 to mGluR8) can act excitatory or inhibitory, depending on associated signal cascades. Expression and localization of inhibitory acting mGluRs at inner hair cells (IHCs) in the cochlea are largely unknown. Here, we analyzed expression of mGluR2, mGluR3, mGluR4, mGluR6, mGluR7, and mGluR8 and investigated their localization with respect to the presynaptic ribbon of IHC synapses. We detected transcripts for mGluR2, mGluR3, and mGluR4 as well as for mGluR7a, mGluR7b, mGluR8a, and mGluR8b splice variants. Using receptor-specific antibodies in cochlear wholemounts, we found expression of mGluR2, mGluR4, and mGluR8b close to presynaptic ribbons. Super resolution and confocal microscopy in combination with 3-dimensional reconstructions indicated a postsynaptic localization of mGluR2 that overlaps with postsynaptic density protein 95 on dendrites of afferent type I spiral ganglion neurons. In contrast, mGluR4 and mGluR8b were expressed at the presynapse close to IHC ribbons. In summary, we localized in detail 3 mGluR types at IHC ribbon synapses, providing a fundament for new therapeutical strategies that could protect the cochlea against noxious stimuli and excitotoxicity.—Klotz, L., Wendler, O., Frischknecht, R., Shigemoto, R., Schulze, H., Enz, R. Localization of group II and III metabotropic glutamate receptors at pre- and postsynaptic sites of inner hair cell ribbon synapses. FASEB J. 33, 000–000 (2019). www.fasebj.org

KEY WORDS: cochlea · mGluR · IHC · mGlu receptor

Within the mammalian cochlea, the mechanosensory hair cells are typically organized into a single row of inner hair cells (IHCs) and 3 rows of outer hair cells (OHCs). Although IHCs are connected predominantly by afferent bipolar type I spiral ganglion neurons that transmit the acoustic information to the brain stem, OHCs mostly contact efferent neurons and are believed to function as cochlear amplifiers (1). Upon stimulation, ribbon synapses of hair cells release the excitatory neurotransmitter glutamate that binds to ionotropic (ion channel–associated) and metabotropic (G-protein–coupled) glutamate receptors.

Ionotropic glutamate receptors preferentially mediate fast excitatory synaptic transmission, whereas metabotropic glutamate receptors (mGluRs) modulate neuronal excitability, synaptic plasticity, and transmitter release (2). The 8 known mGluR types are subdivided into 3 groups: Group I (mGluR1 and mGluR5), group II (mGluR2 and mGluR3), and group III (mGluR4, mGluR6, mGluR7, and mGluR8) (3). Whereas group I receptors positively modulate the activity at glutamatergic synapses, members of group II and III preferentially reduce neurotransmitter release. These diverse functions can be derived from their specific expressions at glutamatergic synapses. Generally, group I receptors are expressed at the postsynapse; members of group II were found both pre- and postsynaptically; and group III mGluR types show a clear preference for the presynaptic terminal (4). An exception is mGluR6; within the CNS, this receptor is expressed exclusively in the retina at postsynaptic sites of ON bipolar cells (5).

Although the cochlear distribution and function of ionotropic glutamate receptors are well described (6, 7), most studies analyzing their metabotropic counterparts focused on the group I receptors mGluR1 and mGluR5

ABBREVIATIONS: 3D, 3-dimensional; 5-HT2A, 5-hydroxytryptamine receptor 2A; CRIP1a, cannabinoid receptor interacting protein 1a; CtBP2/RIBEYE, C-terminal binding protein 2; EM, electron microscopy; HEK, human embryonic kidney; IHC, inner hair cell; mGluR, metabotropic glutamate receptor; OHC, outer hair cell; PFA, paraformaldehyde; PSD95, postsynaptic density protein 95; STED, stimulated emission depletion

[1] Correspondence: Institut für Biochemie, Friedrich-Alexander University Erlangen-Nürnberg, Fahrstrasse 17, 91054 Erlangen, Germany. E-mail: ralf.enz@fau.de

doi: 10.1096/fj.201901543R
This article includes supplemental data. Please visit *http://www.fasebj.org* to obtain this information.

[*e.g.*, see Lu (8)]. Much less is known about receptors belonging to group II (mGluR2 and mGluR3) and group III (mGluR4, mGluR7, and mGluR8) types in the cochlea. One study suggested the presence of group II mGluRs in efferent lateral olivocochlear GABAergic fibers that in turn inhibit efferent dopaminergic signaling onto IHCs (9). Polymorphisms in mGluR7 were correlated with age-related hearing deficits or noise-induced hearing loss in humans (10–13). Furthermore, a general expression of mGluR7 and mGluR8 in IHCs and OHCs was observed, but a synaptic localization of the receptors was not investigated (12, 14). Obviously, a comprehensive study regarding expression and synaptic localization of group II/III receptors in the cochlea is missing.

Therefore, we analyzed the expression of the group II and III mGluR types in the mouse cochlea. In addition, we investigated in detail the distribution of corresponding receptor proteins with respect to the presynaptic ribbon of IHCs in cochlear wholemounts of adult gerbils and mice. Group II and III mGluR types are predestinated to protect against excitotoxic effects caused by overstimulation and excessive glutamate release from IHCs, which could cause neurodegeneration and hearing impairment (15, 16). Thus, our detailed description of group II and III mGluRs at IHC ribbon synapses offers new therapeutical approaches for the treatment of hearing impairments.

MATERIALS AND METHODS

Experiments were carried out in accordance with the guidelines of the University Erlangen-Nürnberg and the Deutsche Forschungsgemeinschaft.

Molecular biology

For RNA isolation, cochleae were dissected from the temporal bone and immediately frozen in liquid nitrogen. Three cochleae of mice (C57BL/6, 6–8 wk) were homogenized using Minilys Personal Homogenizer (Bertin Instruments, Montigny-le-Bretonneux, France) and total RNA was extracted with the RNeasy Micro Kit (Qiagen, Germantown, MD, USA). Genomic DNA was removed by digestion with DNAse, and cDNA synthesis was performed using the QuantiTect Reverse Transcription Kit (Qiagen) and random hexameres-oligo-dT. PCR amplification was performed with 3 μl (40 ng) reverse transcribed RNA in 50 μl of PCR buffer (mM: 20 Tris-HCl, 50 KCl, 2 $MgCl_2$, 0.2 dNTPs), 0.2 pM each primer (see **Table 1**), 10 U Taq-polymerase [(Thermo Fisher Scientific, Waltham, MA, USA), pH = 8.0] in a thermocycler (Thermo Fisher Scientific) using the following parameters: 94°C for 2 min followed by 35 cycles at 94°C for 45 s, 60°C for 60 s, 72°C for 60 s, and a final incubation at 72°C for 10 min. A total of 5 μl of each PCR product was separated on a 1.5% agarose gel. Primer pairs amplify a C-terminal region of the receptor sequences and were designed to span introns to detect residual chromosomal DNA contaminations (Table 1). Primer pairs for mGluR2, 3, 4, 7a, 7b, 8a, and 8b were successfully tested with mouse brain cDNA or with a plasmid sequence for the retina-specific mGluR6 (data not shown). Control amplifications (H_2O) showed no specific PCR products. All PCR amplificates were identified by DNA sequencing.

Immunocytochemistry

For immunofluorescence staining, cochlea of mongolian gerbils or mice were used. Gerbils [MON(Tum)] were between 6 and 8 wk of age and were obtained from Janvier Labs (Le Genest-Saint-Isle, France). Mice (C57BL/6) were between 6 and 12 wk, and they were either purchased (Janvier) or bred in-house. Animals were euthanized, and the cochleae were dissected using a stereomicroscope. Thereafter, 4% paraformaldehyde (PFA) in PBS was applied over the round window. Cochleae of adult gerbils were fixed for 1 h and of adult mice (6–12 wk) for 15 min on ice. Thereafter, the cochlea was opened near the apex and explanted and decalcified in 140 mM EDTA at 4°C overnight. Gerbil cochlea turns were cut into 3 pieces after decalcification. Samples were blocked for 1 h in 5% horse serum and 0.3% Triton X-100 in PBS. Primary antibodies were diluted in 0.1% horse serum, 0.1% Triton X-100 in PBS, and applied overnight at 4°C, as specified in **Table 2**. Secondary antibodies (Alexa Fluor-488–conjugated anti-mouse or rabbit, Cy3 or Alexa Fluor-568–conjugated anti-mouse or guinea-pig, Alexa Fluor-647–conjugated anti-goat or mouse) were diluted, as described previously, supplemented with DAPI and applied for 1 h at room temperature [secondary antibodies were purchased from Thermo Fisher Scientific, Dianova (Pine Bush, NY, USA), or Jackson ImmunoResearch Laboratories (West Grove, PA, USA)]. Finally, samples were mounted with Aqua Poly/Mount (Polysciences, Warrington, PA, USA).

Fluorescent labels were visualized with a Zeiss Axio Imager Z2 (Carl Zeiss, Oberkochen, Germany) equipped with an

TABLE 1. *Oligonucleotides used for expression analysis*

	Oligonucleotide, 5′−3′	
Gene	P1	P2
mGluR2	CAGTGATTATCGGGTGCAG	TCAAAGCGACGATGTTGTTGAG
mGluR3	TACACCACCTGCATCATCTG	TCACAGAGATGAGGTGGTGG
mGluR4	CGGCTGACAAGCTGTACATC	CTAGATTGCATGGTTGGTGTAAG
mGluR6	GTATTATCTGGCTGGCTTTCG	CTACTTGGCGTCCTCTGAGTTC
mGluR7a/b	CACCCTGAACTCAATGTCCAG	
mGluR7a		TTAGATAACCAGGTTATTATAACTG
mGluR7b		CTATACTGTTGGTGGGATAGTG
mGluR8a/b	CACGTGCATCATTTGGTTAGC	
mGluR8a		TCAGATTGAATGATTACTGTAGC
mGluR8b		TTAGGAAGTGCTCCCGCTC

Overview of DNA sequences of used oligonucleotides. Primers amplify a C-terminal region of the receptor sequences and span an intron to detect potential amplification of chromosomal DNA. (P1, sense primer; P2, antisense primer, stop codons in the antisense primers are underlined).

TABLE 2. *Primary antibodies used in this study*

Protein	Epitope	Dilution	Serum type	Antibody no./supplier	Reference
Bassoon	rat Bassoon	1:400	mouse monoclonal	ADI-VAM-PS003/ Enzo Life Sciences, Farmingdale, NY, USA	
CtBP2/RIBEYE	mouse aa 361-445	1:300	mouse monoclonal	612044/ BD Biosciences, San Jose, CA, USA	
CtBP2/RIBEYE	rat aa 974-988	1:5000	rabbit polyclonal	192003/ Synaptic Systems, Göttingen, Germany	
CtBP2/RIBEYE	rat aa 95-207	1:5000	guinea-pig polyclonal	192104/ Synaptic Systems	
mGluR2/3	rat mGluR2 aa 860-872	1:100	rabbit polyclonal	AB1553/ Merck Millipore, Burlington, MA, USA	
mGluR2	NT seq. of 47 aa	1:150	mouse monoclonal	AB15672/ Abcam, Cambridge, MA, USA	
mGluR3	NT seq. of 16 aa	1:150	rabbit polyclonal	AB188750/ Abcam	
mGluR4	rat aa 834-912	1:150	rabbit polyclonal		18
mGluR8	human aa 34-514	1:50	mouse monoclonal	MAB5277/R&D Systems, Minneapolis, MN, USA	
mGluR8a	rat aa 886-908	1:1000	guinea-pig polyclonal	AB5362/MilliporeSigma, Burlington, MA, USA	
mGluR8b	mouse aa 886-908	1:150	rabbit polyclonal		19
PSD95	mouse aa 64-247	1:250	mouse monoclonal	124011/Synaptic Systems	
PSD95	mouse aa 1-100	1:100	goat polyclonal	AB12093/Abcam	
Shank 2	rat aa 1042-1475	1:1000	rabbit polyclonal	162202/Synaptic Systems	
Shank 2	rat aa 1042-1475	1:5000	guinea-pig polyclonal	162204/Synaptic Systems	
Synapsin 1	mouse aa 445-462	1:1000	guinea-pig polyclonal	106104/Synaptic Systems	

Overview of primary antibodies used in this study. The epitope is characterized by species and amino acid region, if known. NT seq., N-terminal sequence.

ApoTome by using Zen blue 2012 software. Images were taken with a ×63 objective (1.4 oil, Apochromat; Carl Zeiss), and *z* projections were calculated with Zen software (Carl Zeiss). To study 3-dimensional (3D) protein distributions, images were taken with a laser scanning microscope (LSM 710; Carl Zeiss) equipped with a ×63 objective. A total of 4 excitation laser wavelengths were used (405, 488, 561, and 633 nm) between 0.8 and 4% intensity. *Z* stacks were recorded with the corresponding imaging modules under the same settings, with a stack interval of 0.9 μm and a pinhole of 1 airy unit by using Zen black 2010 software. The 3D images were reconstructed from *z* stacks using Imaris 8 (Bitplane, Belfast, United Kingdom).

For high-resolution stimulated emission depletion (STED) microscopy, anti-rabbit Star-580 1:200 and anti-mouse Star-635P 1:200 (Abberior Instruments, Göttingen, Germany) were used as secondary antibodies and probes were mounted with mowiol dabco (MilliporeSigma, Burlington, MA, USA). Thereafter, cochlea wholemounts were analyzed with a STED microscope (2-Channel Super Resolution Microscope; Abberior Instruments) equipped with a ×100 oil immersion lens (NA: 1.44). Probes were excited at 594 and 640 nm, and STED was performed at 775 nm with a pulsed laser (total laser power 1250 mW used at 50%). Before sample recording, proper alignment of both excitation lasers was controlled using TetraSpeck Microspheres (Thermo Fisher Scientific). In addition, laser alignment and chromatic aberrations of the optical array were monitored by STED as follows: the STED beam was guided through a spatial light modulator to create phase patterns required for 2D and 3D STED microscopy, which corrects optical aberrations at the same time. Because emitted fluorescence is confined to the intensity center of the STED beam, using 1 STED beam for both dyes assures that minor misalignments of the excitation beams would not be present in the recorded images. All images were acquired using Imspector Software (Abberior Instruments) in 3D STED mode with an *xyz* pixel size from 20 × 20 × 38.25 nm and a resolution in *xyz* of 90 nm, using identical laser power, gain, and microscope settings. Deconvolution was performed in Huygens Professional 18.04 (Scientific Volume Imaging, Hilversum, The Netherlands), and images were reconstructed from *z* stacks using Imaris 8 (Bitplane).

All antibody incubations of mouse cochlear wholemounts were repeated between 3 and 6 times, except incubations (see Fig. 3). As control, cochleae were incubated with secondary antibodies only, which resulted in the absence of detectable fluorescence. Recorded fluorescent signals were assembled in Adobe Photoshop (CS5; Adobe Systems, San Jose, CA, USA) and contrast enhanced and enlarged, if needed for better visualization.

Cell culture

The specificity of immune sera directed against mGluR2, mGluR3, mGluR8a, and mGluR8b was verified with human embryonic kidney (HEK)-293 cells transfected with plasmids encoding the receptors. HEK-293 cells were grown in 6 well plates at 37°C and 5% CO_2 on glass coverslips coated with poly(L-lysine)/3-aminopropyltriethoxysilane in minimum essential medium that were supplemented with 10% fetal bovine serum, L-glutamine, and penicillin and streptomycin (Thermo Fisher Scientific) to ~50% confluency. Cells were transfected with 2 μg plasmid DNA encoding for the rat sequences of mGluR2 or mGluR3 (kindly provided by J.-P. Pin, Institut de Genomique Fonctionnelle, Montpellier, France) and mGluR8a or mGluR8b (kindly provided by F. Ferraguti, Innsbruck, Austria) for 18 h using lipofection (jetPEI; Polyplus-transfection, New York, NY, USA). Thereafter, cells were washed 3 times with PBS and incubated for another 48 h as above to allow protein expression. Then, cells were washed, fixed in 4% (v/v) PFA/PBS for 10 min on ice, washed again, and blocked with 10% (v/v) fetal bovine serum containing 2% (w/v) bovine serum albumine and 0.1% Triton X-100 for 30 min. Subsequently, cells were incubated for 1.5 h at room temperature with primary antibodies diluted in blocking solution, as indicated in Supplemental Figs. S2 and S3 (see Table 2 for details of the used immune sera). After washing, secondary antibodies (Alexa Fluor-488–conjugated anti-mouse or rabbit, Cy3-conjugated anti-mouse or rabbit) together with DAPI were diluted as above and applied for 45 min at room temperature.

All immune sera recognizing the different mGluR types analyzed in this study were also tested on neurons. Dissociated cortical neurons were prepared from E18 Sprague-Dawley rats in HBBS as previously described in Valenzuela *et al*. (17). In brief, the cortex (excluding olfactory bulb and hippocampus) was dissected, washed in HBBS ($-Ca^{2+}$, $-Mg^{2+}$), and incubated in HBBS containing papain for 5 min (37°C). Following papain treatment, cells were washed in HBBS ($+Ca^{2+}$, $+Mg^{2+}$) and carefully dispersed in DMEM supplemented with 10% fetal calf serum. Cells were plated on poly(L-lysine)-coated 12-mm cover slips in a 24-well plate at a density of 100×10^3 cells/ml. Cultures were maintained in serum-free neurobasal medium containing B27 supplement (Thermo Fisher Scientific) and kept at 37°C in 5% CO_2.

After 14–21 d in culture, cells were washed, fixed in 4% PFA/PBS for 10 min on ice, and incubated with immune sera recognizing the mGluR types indicated in Supplemental Fig. S1 and the postsynaptic marker protein Shank 2 (see Table 2 for antibody specifications) for 1.5 h at room temperature. The binding sites of the primary antibodies were visualized by secondary antibodies coupled to Alexa Fluor-488–conjugated rabbit, Alexa Fluor-568–conjugated anti-guinea-pig (Thermo Fisher Scientific). Coverslips containing stained cortical neurons were extensively washed and mounted with Aqua Poly/Mount (Polysciences). Fluorescent signals of stained HEK-293 cells and of cortical neurons were recorded with a Zeiss Axio Imager Z2 (Carl Zeiss) and assembled in Adobe Photoshop (Adobe Systems), as described above. As control, cells were incubated with a mixture of only secondary antibodies, which resulted in the absence of detectable signals.

Data analysis

The ImageJ tool Plot Profile was used to measure fluorescence profiles in individual confocal images (ImageJ v.1.49g; National Institutes of Health, Bethesda, MD, USA). The 3D reconstructions of fluorescent signals of *z* stacks from STED or confocal microscopy, the definition of the centers of gravity of reconstructed signals, as well as distance and angle measurements were performed with Imaris (Bitplane). Obtained data sets were evaluated using the Microcal Origin Software (Microcal Software, Northampton, MA, USA). Statistical significance was calculated with the 1-way ANOVA test. Errors are expressed as means ± SD.

RESULTS

Group II and group III mGluRs are expressed in the mouse cochlea

Several studies describe functions of group I mGluRs (mGluR1 and mGluR5) in the cochlea [*e.g.*, see Lu (8)]. However, there are no comprehensive studies regarding expression of group II and III receptors in this tissue. Therefore, we analyzed in detail expression and localization of group II (mGluR2, mGluR3) and group III (mGluR4, mGluR6, mGluR7, mGluR8) receptors in the cochlea of a mouse and gerbil.

To pave the ground for successive anatomic studies, we first tested the presence of group II and III mGluR types in the mouse cochlea, including common splice variants. **Figure 1** shows specific PCR amplificates for mGluR2, mGluR3, and mGluR4 and for the receptor isoforms mGluR7a, mGluR7b, mGluR8a, and mGluR8b. MGluR6 was not detectable in the cochlea, which is in line with its specific expression in bipolar cells of the retina within the CNS (5).

Next, we analyzed the distribution of cochlear group II and III mGluRs with respect to the ribbon synapse of IHCs. Our studies were guided by the quality and specificity of available immune sera. We used antibodies, recognizing a conserved epitope in mGluR2 and mGluR3, in the following designated mGluR2/3, antibodies specific for mGluR2, mGluR3, mGluR4, and immune sera detecting mGluR8a or mGluR8b isoforms. Antibodies for mGluR2/3, mGluR4, mGluR8a, and mGluR8b were well characterized and used before by several groups, including ourselves, and thus are supposed to be specific (18–20). Nevertheless, we again tested the quality of the immune-sera using primary cultures of cortical neurons and antibodies binding Shank 2 to label postsynaptic sites (Supplemental Fig. S1). The immune serum used in the past to detect mGluR7 in neuronal tissue [*e.g.*, the retina (21] is not available anymore. Because currently available immune sera cannot reproduce the original data, mGluR7 was omitted from our studies.

Group II mGluR types show a synaptic expression in cochlear wholemounts

The antibodies recognizing a conserved epitope in the group II receptors mGluR2 and mGluR3 (mGluR2/3) bind to a linear stretch of amino acids conserved in their C-termini, preventing a distinction between these 2

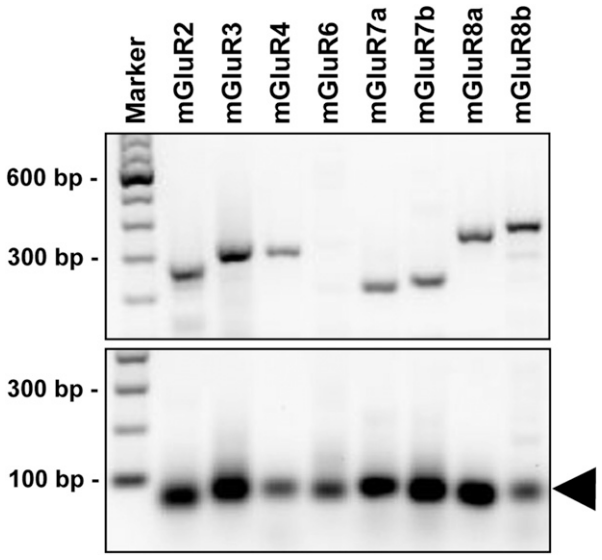

Figure 1. Expression of group II and III mGluR types in the mouse cochlea. Top: agarose gel showing PCR amplificates of expected size for the indicated mGluR types obtained from reverse transcribed transcripts purified from mouse cochlea. Expressions of prominent C-terminal splice variants of mGluR7 and mGluR8, termed a and b, were analyzed individually. The identity of PCR products was verified by sequencing. Bottom: negative controls (H_2O) show primer-dimer formations (arrowhead) but no amplificates of the expected sizes. The left lane shows a 100-bp marker. For better visualization, black and white levels of the original photograph were inversed.

mGluR types. Although mGluR2- or mGluR3-specific antibodies are available, these sera are less characterized. Therefore, we performed all initial studies involving 3D reconstructions with the reliable mGluR2/3 serum, whereas the identity of the group II mGluR type was determined in separate stainings using antibodies specific for mGluR2 or mGluR3.

Gerbils are a well-studied animal model in hearing research. Thus, we marked presynaptic sites of IHCs in cochlear wholemounts of the gerbil by antibodies specific for C-terminal binding protein 2 (CtBP2/RIBEYE), the main protein of synaptic ribbons (22). Colabeling the same tissue for mGluR2/3 resulted in a punctate label that was always observed in close vicinity to the CtBP2-positive presynaptic ribbon of IHCs (**Fig. 2*A, B***). Given the prominent signal intensity for mGluR2/3, we next analyzed the distribution of the receptors in the much smaller mouse cochlea (Fig. 2*C, D*). Comparing the spatial distribution of the relative signal intensities obtained for mGluR2/3 and CtBP2 showed a partial overlap of both signals (Fig. 2*b′b″*, *d′d″*). This observation would be consistent with 2 possible localizations of mGluR2/3 relative to the synaptic cleft: *1*) a presynaptic expression outside the active zone, or *2*) a postsynaptic expression of mGluR2/3 opposite to the presynaptic ribbon.

Signals for mGluR2/3 are present at postsynaptic sites of IHC ribbon synapses

Because the mGluR2/3 staining patterns were comparable between the gerbil and mouse, we used mouse tissue only in the following. To distinguish between a pre- *vs.* postsynaptic expression of mGluR2/3 at IHC synapses, we analyzed the receptors' distribution in more detail using STED microscopy. Cochlear wholemounts from mice were costained with antibodies recognizing mGluR2/3 and the CtBP2/RIBEYE immune serum used above, which marks the presynaptic ribbon (**Fig. 3*A–E***). To stain postsynaptic specializations formed by afferent type I spiral ganglion neurons that are located opposite to the presynaptic ribbon, we used antibodies recognizing the postsynaptic density protein 95 (PSD95) (23) (Fig. 3*A, F–H*). Z-stacks obtained from dual-color STED microscopy were 3D reconstructed and distances from the centers of gravity were measured, as exemplified by the dots shown in Fig. 3*C, F*. Whereas the mean distance between mGluR2/3 and presynaptic ribbons was between 138 and 428 nm (mean of 258 ± 88.6 nm), the distance between the receptors and PSD95 was significantly smaller (81.8 ± 31.0 nm; Fig. 3*I*). These data favor a postsynaptic expression of mGluR2/3, slightly displaced from the PSD95-labeled postsynaptic density.

In order to strengthen this assumption, we labeled simultaneously pre- and postsynaptic terminals using the marker antibodies shown in **Fig. 4*A*** and compared resulting fluorescent signals with the expression of mGluR2/3. Unfortunately, the available STED microscope allowed the simultaneous detection of 2 color channels only. Therefore, we switched back to classic confocal microscopy in combination with 3D reconstruction. Cochlear wholemounts of mice were incubated with antibodies binding to mGluR2/3, CtBP2/RIBEYE, and PSD95, and the geometry of individually labeled synapses was 3D reconstructed from the confocal images (Fig. 4*A, B*). Reconstructions of the CtBP2/RIBEYE label showed that the size of the presynaptic ribbons was elongated into 1 direction, a feature that was observed by other groups before (24). This is represented in Fig. 4*C, D*, which compare the same synapse horizontally rotated by about 90°. Examples of more ribbon synapses are summarized in Fig. 4*E*. In all synapses analyzed, we observed a clear overlap of mGluR2/3 with the postsynaptic marker PSD95, which was clearly separated from the presynaptic CtBP2/RIBEYE–labeled ribbon.

Interestingly, mGluR2/3 was not completely colocalized with PSD95, but it was always slightly displaced. PSD95 marks the active zone within synapses that contains α-amino-3-hydroxy-5-methyl-4-isoxazolepropionic acid (AMPA)-type glutamate receptors, whereas mGluR2/3 seem to be expressed just adjacent to the release site of glutamate. To quantify these observations, we calculated the centers of gravity for reconstructed signals of CtBP2/RIBEYE, PSD95, and mGluR2/3 at more than 40 individual

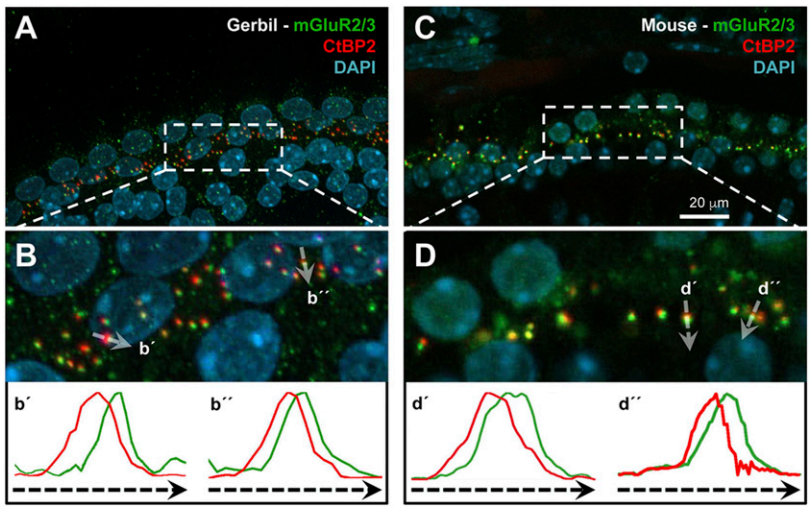

Figure 2. Localization of mGluR2/3 in cochlear wholemounts of a gerbil and mouse. *A*) Confocal micrograph showing a cochlear wholemount from gerbil that was incubated with antibodies recognizing CtBP2/RIBEYE (red) to label the ribbon in presynaptic hair cell terminals and with DAPI (cyan) to visualize cellular nuclei. Costaining with an immune serum recognizing a conserved epitope in mGluR2 and mGluR3 (mGluR2/3, green) resulted in a punctate staining pattern in close vicinity to presynaptic ribbons. This is best seen in the magnification of the boxed region shown in the lower panel (*B*). The intensity of green and red fluorescent signals was measured along the white transparent arrows and compared in *b′* and *b″*. *C, D, d′, d″*) Cochlear wholemounts from a mouse were stained and analyzed as previously described.

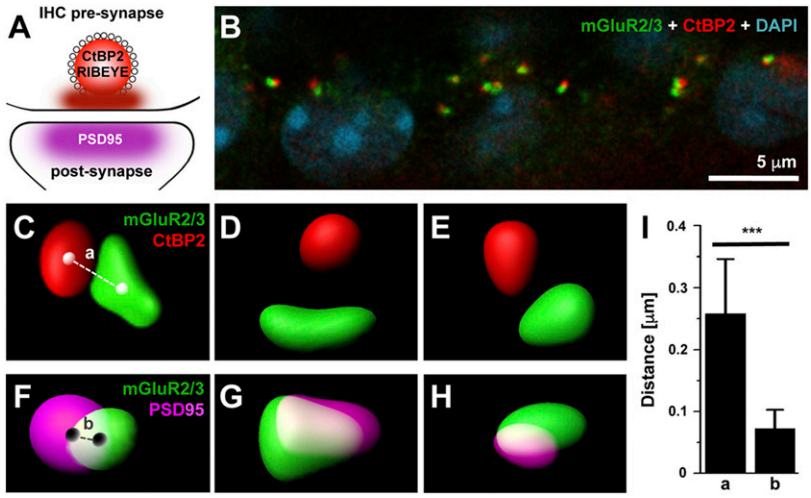

Figure 3. Staining for mGluR2/3 overlaps with postsynaptic but not with presynaptic markers. *A*) Sketch of an IHC ribbon synapse depicting the distribution of used marker proteins relative to the synaptic cleft: CtBP2/RIBEYE labels the presynaptic ribbon (red) that is surrounded by glutamatergic vesicles (white circles), whereas PSD95 (magenta) serves as a postsynaptic marker. *B*) STED image of a cochlear wholemount from a mouse incubated with antibodies recognizing mGluR2/3 (green) and CtBP2/RIBEYE (red) and DAPI to mark cellular nuclei, as analyzed by dual-color STED microscopy. *C*) The geometry of fluorescent signals was 3D reconstructed, centers of gravity for green and red labels were calculated (white balls), and their distances were measured (dashed line; *a*). *F*) Similar analysis as in (*C*), using the postsynaptic marker PSD95 (magenta) to measure distances, as indicated (black circles; *b*). *D, E, G, H*) More examples of reconstructed signals. *I*) Bar diagram comparing measured distances between mGluR2/3 and CtBP2/RIBEYE ($n = 8$; *a*), or between mGluR2/3 and PSD95 ($n = 6$; *b*). The number of synapses analyzed is indicated in white. $^{***}P < 0.0005$.

ribbon synapses, represented by white dots as shown in Fig. 4*D*. The mean distance between the pre- and postsynaptic markers CtBP2/RIBEYE and PSD95 (274 ± 89.0 nm) was comparable to the distance between CtBP2 and mGluR2/3 (279 ± 86.1 nm; Fig. 4*F*). In contrast, the mean distance between PSD95 and mGluR2/3 was significantly shorter (164 ± 32.2 nm), indicating that these 2 proteins are localized at the same side of the synaptic cleft. Calculating the angles between the 3 centers of gravity showed similar values for β (74.0 ± 19.8°) and γ (71.4 ± 22.8°; Fig. 4*F*) that were significantly different from α (34.6 ± 10.8°), being consistent with a postsynaptic localization of mGluR2/3.

Next, we exchanged CtBP2/RIBEYE with Bassoon as another presynaptic marker that is involved in anchoring the ribbon to the presynaptic membrane (Fig. 4*A*) (24, 25). Label for mGluR2/3 did overlap with PSD95, but not with Bassoon (Fig. 4*G*). Measuring distances and angles between the centers of gravity of signals obtained from several synapses suggested that mGluR2/3 are present in close vicinity to PSD95 (mean of 140 ± 24.8 nm) while being significantly more distant to Bassoon (mean of 272 ± 104 nm) (Fig. 4*H*). As before, the closest angle was α (34.3 ± 15.9°), being significantly smaller than β (66.9 ± 21.2°) or γ (78.8 ± 17.1°). Our data are consistent with mGluR2/3 being localized at the same side of the synaptic cleft as

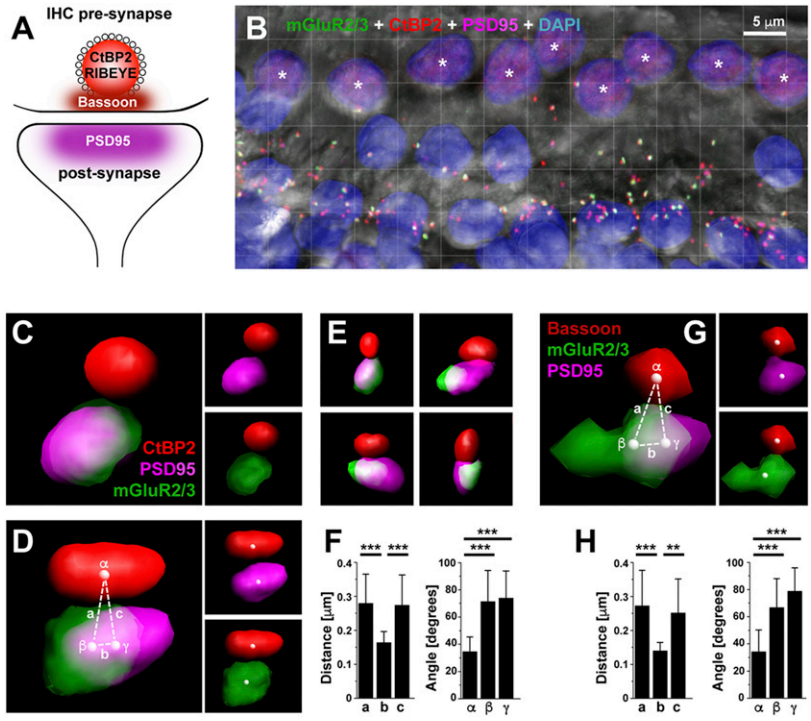

Figure 4. Signals for mGluR2/3 are located at the IHC postsynapse, adjacent to the active zone. *A*) Sketch of an IHC ribbon synapse showing the locations of presynaptic (CtBP2/RIBEYE: red; Bassoon: dark red) and postsynaptic (PSD95: magenta) marker proteins relative to the synaptic cleft. *B*) Overview of a 3D stack of confocal images from a cochlear wholemount of a mouse that was incubated with antibodies recognizing the proteins indicated, or DAPI to mark cellular nuclei. The CtBP2/RIBEYE immune serum cross-reacts with IHC nuclei (asterisks). The background shows the same region in phase contrast (gray). *C*) Reconstruction of the 3D geometry of fluorescent signals, as indicated. To visualize the distance between different labels more clearly, individual color combinations are shown separately in the small panels to the right. *D*) Represents the same synapse as in *C*, rotated horizontally by ~90°. A 360° rotation of this synapse is shown in the Supplemental Movie. For each color, the center of gravity (white dots) was calculated, and distances (a, b, c) and angles (α, β, γ) were measured, as indicated. *E*) More reconstructed synapses, labeled as indicated in *C*. *F*) Bar diagrams summarizing calculated mean distances and angles between the centers of gravity of 42 synapses as shown in *D*. White numbers represent the synapse quantity analyzed. *G, H*) Reconstruction and measurements of 13 3D reconstructed synapses, as in *D* and *F*, using Bassoon as presynaptic marker. $^{**}P < 0.005$, $^{***}P < 0.0005$.

PSD95. We conclude that mGluR2/3 is expressed at the postsynaptic side of IHC ribbon synapses, directly adjacent to the active zone.

Expression of mGluR2/3 does not change along the tonotopic axis

It has been shown that the number of ribbon synapses per IHC varies along the tonotopic axis in the cochlea of a mouse and gerbil (26). Therefore, we asked if the expression of mGluR2/3 at these synapses might also change along the spectral gradient. To this end, we costained cochlear wholemounts of mice for CtBP2/RIBEYE and mGluR2/3, as above. Three different tonotopic locations of the cochlea (apex, middle, and base) were selected, and the number of fluorescent puncta representing CtBP2/RIBEYE or mGluR2/3 were counted, as indicated in **Fig. 5*A–C***. Finally, the number of mGluR2/3-positive puncta obtained from the individual micrographs was normalized to the number of detected IHC ribbons. Figure 5*D* shows that we detected mGluR2/3-specific signals at 94–98% of IHC ribbon synapses, and that these numbers did not change significantly along the tonotopic axis.

MGluR2/3-specific signals are not present at efferent terminals contacting IHC synapses

Previously, mGluR2/3 were proposed to be expressed by GABAergic neurons that inhibit dopaminergic terminals (9). Although expression of these receptors was not detected directly, the authors suggested that group II mGluRs could be activated by a spill-over of glutamate released from the nearby IHC ribbon synapse. This, in turn, would reduce the release of GABA, leading to a disinhibition in dopaminergic terminals. Thus, we tested if the lateral shift observed in the localization of mGluR2/3 in respect to PSD95 (see Figs. 3*F–I* and 4*C–H*) could be explained by the expression of the receptors in efferent terminals contacting the IHC ribbon synapse, rather than being present at the afferent IHC postsynapse. To this end, we marked olivocochlear efferent terminals with antibodies recognizing Synapsin 1 (27). Costaining cochlear wholemounts from mice for mGluR2/3, Synapsin 1, CtBP2/RIBEYE, and PSD95 in different combinations did not show any obvious colocalization of the receptors with Synapsin 1–labeled efferent terminals (**Fig. 6**). Although we cannot rule out a low expression level at olivocochlear efferent terminals, we conclude that the majority of mGluR2/3 is present at the IHC postsynapse.

MGluR2, but not mGluR3, can be detected at IHC ribbon synapses

The mGluR2/3 immune serum used in this study was generated against a C-terminal sequence from mGluR2 that is highly conserved in mGluR3. Because we detected transcripts for both group II receptors in the cochlea (see Fig. 1), we next investigated if both receptors would be actually present at IHC synapses, using receptor-specific antibodies. Because the mGluR2- and mGluR3-specific immune sera are not used to the same extend in the scientific literature as the well-established mGluR2/3 serum, we ensured that the antibodies would be receptor specific and able to bind to the native receptor epitope in neurons, using HEK-293 cells and cortical neurons in culture (Supplemental Figs. S1 and S2).

Costaining of cochlear wholemounts for CtBP2/RIBEYE, mGluR2, or mGluR3 showed that only signals derived from the mGluR2/3 and mGluR2 sera were detectable in close vicinity to IHC ribbons (**Fig. 7*A–D***). In contrast, mGluR3 fluorescence appeared more diffuse and was not colocalized with synaptic ribbons (Fig. 7*E*). Given the lower intensity of mGluR3-specific signals in the cochlea, we tested this serum on cortical neurons, as mentioned in the previous paragraph. Colabeling synapses for the postsynaptic marker protein Shank 2 showed a colocalization with the binding sites of the mGluR3 antibodies (Fig. 7*F*), indicating that the serum is able to recognize the native receptor epitope in a neuronal context. This observation is in agreement with previous studies that described mGluR3 in primary cultures of cortical neurons (28, 29). These data suggest that mGluR2, but not mGluR3, is present at the postsynaptic side of IHC ribbon synapses.

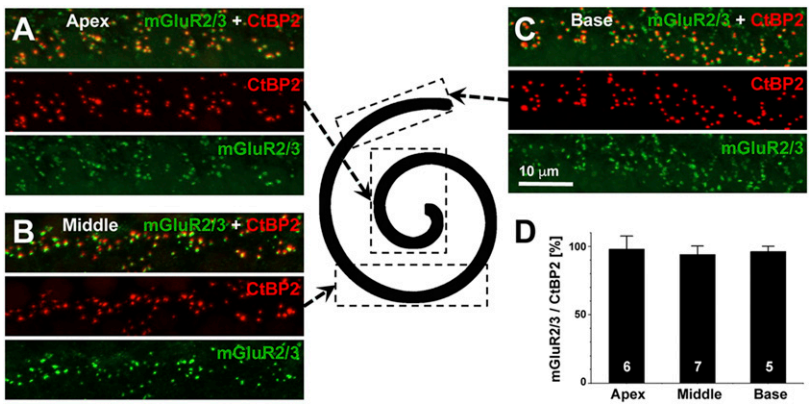

Figure 5. The relation between mGluR2/3 clusters and IHC ribbons remains constant along the tonotopic axis. Cochlear wholemounts from a mouse were incubated with antibodies recognizing mGluR2/3 (green) and CtBP2/RIBEYE (red). *A–C*) Confocal images were taken from 3 regions indicated by the dashed boxes in the cochlear sketch shown in the middle, representing high (apex; *A*), middle (middle; *B*), or low (base; *C*) frequencies. The number of green clusters (representing mGluR2/3) was counted and normalized to the number of red clusters, representing IHC ribbons. *D*) Bar diagram comparing the number of mGluR2/3-positive clusters with the number of stained IHC ribbons. No statistically significant differences were observed. The number of analyzed pictures for each cochlear region is given in white.

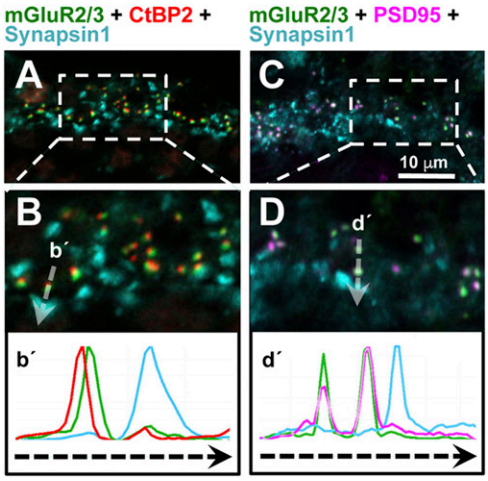

Figure 6. Synapsin 1–positive efferent terminals do not express mGluR2/3. Confocal micrographs of cochlear wholemounts from a mouse incubated with the immune sera were indicated. Olivocochlear efferent terminals were marked with antibodies recognizing synapsin1. *A*) Although signals representing mGluR2/3 (green) and the presynaptic marker CtBP2/RIBEYE (red) are in close vicinity, label for Synapsin 1 (cyan) was observed at different locations. *B*) To compare the distribution of fluorescent signals, the boxed region was enlarged, and intensity profiles were measured along the white transparent arrow and are shown in the lower panel (*b′*). *C*) Micrographs analyzed as in *A*, using the postsynaptic marker PSD95 (magenta) instead of CtBP2/RIBEYE. *D*) As before, signal locations are compared along the transparent arrow and visualized in the lower panel (*d′*).

MGluR4 and mGluR8b are expressed at the presynaptic side of IHC ribbon synapses

Finally, we analyzed the localization of mGluR4, mGluR8a, and mGluR8b in the cochlea. Immune sera for mGluR4 and mGluR8b were demonstrated before to specifically recognize their target proteins (18, 19). Here, we tested if the mGluR8a serum would be reliable as well. Using HEK-293 cells and cortical neurons in culture, we showed that the mGluR8a antibodies do not bind to mGluR8b and that they recognize the native receptor epitope in neurons (Supplemental Figs. S1 and S3).

These immune sera were then applied to cochlear wholemounts, and pre- and postsynaptic specializations were marked for CtBP2/RIBEYE and PSD95 as before. Fluorescent signals representing the different mGluR types appeared as puncta, indicating a synaptic localization of these receptors (**Figs. 8*A*, 9*A*, *B***). However, only mGluR4 and mGluR8b, but not mGluR8a, were in close vicinity to CtBP2/RIBEYE and PSD95. Interestingly, in contrast to the partial overlap of mGluR2/3 with the presynaptic ribbon at IHC ribbon synapses shown in Fig. 4, signals representing mGluR4 or mGluR8b are completely superimposed with the presynaptic ribbon marker CtBP2/RIBEYE (Figs. 8*B* and 9*C*), whereas they overlap only partially with the postsynaptic PSD95 (Figs. 8*C* and 9*D*). This suggested a presynaptic localization of the 2 receptors at IHC ribbon synapses.

Indeed, after reconstructing the geometry of the labeled proteins at individual synapses, we observed a clear overlap of mGluR4 and mGluR8b with the presynaptic CtBP2/RIBEYE–labeled ribbon, whereas the receptors were more distant to the postsynaptic marker PSD95 (Figs. 8*D*, *E* and 9*E*, *F*). As before, the centers of gravity of the reconstructed fluorescent labels representing the receptors, CtBP2/RIBEYE, or PSD95 were calculated for individual ribbon synapses, and distances and angles between these centers were measured, as indicated in Figs. 8*D* and 9*E*. The mean distance between mGluR4 or mGluR8b and the presynaptic marker CtBP2/RIBEYE was significantly shorter (mGluR4: 108 ± 23.4 nm; mGluR8b: 119 ± 54.5 nm) than the distance between the receptors and the postsynaptic label (mGluR4: 373 ± 123 nm; mGluR8b: 317 ± 53.9 nm; Figs. 8*F* and 9*G*). Comparing the angles between the 3 centers of gravity revealed the smallest number at the gravity center for PSD95 (mGluR4: 14.7 ± 9.1°; mGluR8b: 20.5 ± 10.8°; Figs. 8*G* and 9*H*). These data are consistent with a presynaptic localization of mGluR4 and mGluR8b.

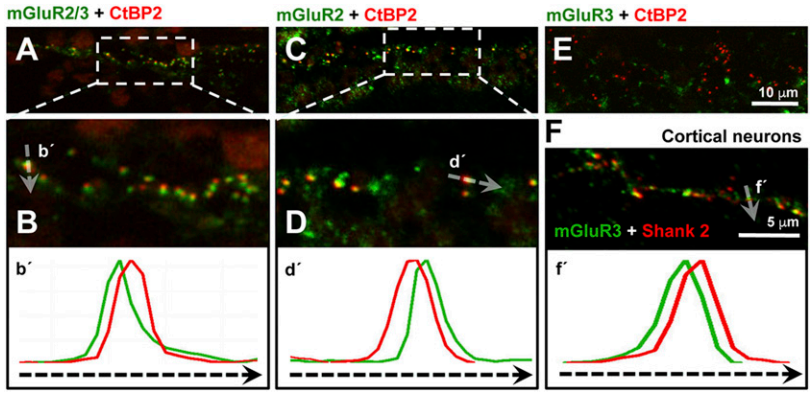

Figure 7. MGluR2, but not mGluR3, is located at the IHC postsynapse. Confocal micrographs of mouse cochlear wholemounts incubated with antibodies binding CtBP2/RIBEYE (red) to mark presynaptic ribbons of IHCs, and with immune sera recognizing mGluR2/3 (*A*), mGluR2 (*C*), or mGluR3 (*E*) (all in green). Fluorescent signals representing mGluR2/3 and mGluR2 were always located at the IHC ribbon synapse. This can be best seen in the enlargements of the boxed regions shown in (*B*, *D*). Intensities of fluorescent signals were measured along the transparent arrows and compared in the lower panels (*b′*, *d′*). In contrast to mGluR2, the mGluR3 immune sera showed a more diffuse staining of low intensity within the region of IHC ribbon synapses. To ensure that these antibodies would recognize the native epitope of mGluR3, we costained primary cortical neurons for mGluR3 (green) and the synaptic marker protein Shank 2 (red) (*F*). Signal intensities were measured along the white arrow, and resulting profiles are compared in *f′*. An enlargement from the Supplemental Fig. S1 is shown in *F*.

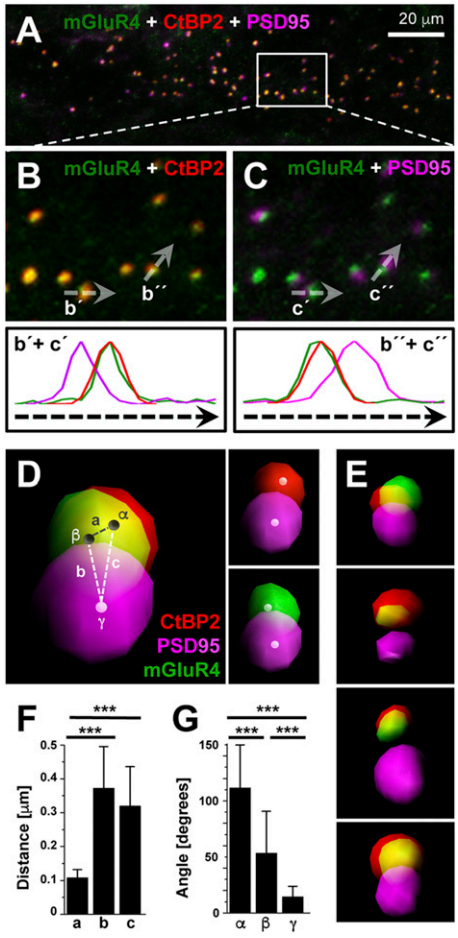

Figure 8. MGluR4 is located at the presynaptic side of IHC ribbon synapses. *A*) Confocal micrograph of a mouse cochlear whole-mount incubated with antibodies labeling presynaptic CtBP2/RIBEYE (red) and postsynaptic PSD95 (magenta) marker proteins and costained with an immune sera recognizing mGluR4 (green). *B*, *C*) The enlargements of the boxed region show a perfect superimposure of signals representing mGluR4 and CtBP2/RIBEYE (*B*), whereas fluorescent labels for mGluR4 and PSD95 were displaced (*C*). This can be best seen in the comparisons of the signal intensities measured along the transparent white arrows ($b' + c'$, $b'' + c''$). *D*) The 3D geometry of fluorescent signals was reconstructed and shown, as described in Fig. 4*C*. *E*. More reconstructed synapses, labeled as in *D*. At individual synapses the centers of gravity were calculated for each fluorescent label (black and white dots) and distances and angles were measured, as indicated. *F*, *G*) Calculated mean distances (*a*, *b*, *c*) and angles (α, β, γ) between the centers of gravity of nineteen 3D reconstructed synapses are summarized in the bar diagrams. White numbers represent the synapse number analyzed. ***$P < 0.0005$.

DISCUSSION

In sensory organs like retina and cochlea, the intensity of a given stimulus is encoded by the graded amount of the neurotransmitter glutamate released at ribbon synapses of photoreceptors or IHCs, respectively. Although expression and function of the inhibitory group II and III mGluR types at the photoreceptor ribbon synapse is well described (30, 31), much less information is available for the ribbon synapse of IHCs. Here, we analyzed the expression and localization of group II and III mGluRs in cochlear wholemounts in respect to the presynaptic ribbon of IHCs.

We identified transcripts encoding mGluR2, mGluR3, mGluR4, as well as common mGluR7 and mGluR8 isoforms in the mouse cochlea. Furthermore, we localized mGluR2, mGluR4, and mGluR8b proteins at pre- or postsynaptic sides of the IHC ribbon synapse. Originally, we intended to analyze the synaptic expression of

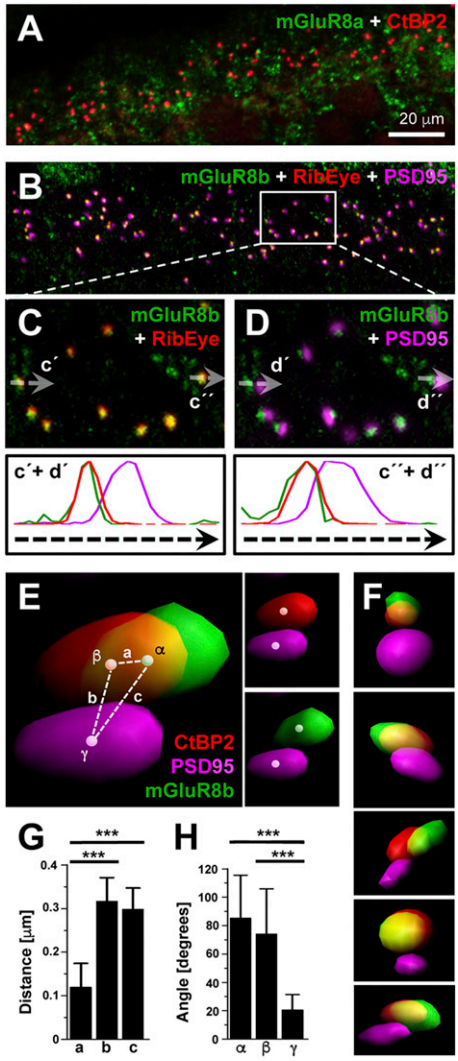

Figure 9. IHC ribbon synapses express mGluR8b, but not mGluR8a. *A–D*) Confocal micrograph of cochlear whole-mounts from a mouse incubated with immune sera recognizing mGluR8a (*A*) or mGluR8b (*B*), together with antibodies binding to pre- or postsynaptic marker proteins, as indicated. Although mGluR8a (green) was not colocalized with the presynaptic ribbon marker CtBP2/RIBEYE (red), mGluR8b showed a perfect overlap with IHC ribbon synapses. This can be best seen in the 2 enlargements of the boxed region that compare the localization of mGluR8b (green) with the presynaptic marker protein CtBP2/RIBEYE (red) (*C*), or with the postsynaptic marker PSD95 (magenta) (*D*). Comparing signal intensities for all 3 colors as measured along the white transparent arrows shows colocalization of mGluR8b with CtBP2/RIBEYE, whereas signals representing PSD95 are displaced ($c' + d'$, $c'' + d''$). *E–H*) The 3D geometry of fluorescent signals of 19 synapses was reconstructed, their centers of gravity were calculated, and distances (*a*, *b*, *c*) and angles (α, β, γ) were measured and graphically compared in bar diagrams, as explained in Fig. 8. ***$P < 0.0005$.

mGluR2, mGluR4, and mGluR8b in detail using electron microscopy (EM). However, multiple efforts to identify proper experimental conditions for immuno EM in the cochlea of gerbils and mice were not successful. Interestingly, we did not find publications describing the localization of proteins at the IHC ribbon synapse in mice older then 21 d by EM techniques, probably pointing to principle experimental difficulties under these conditions. The composition of the neurotransmitter system at the IHC ribbon synapse is transiently modulated by medial olivocochlear efferent fibers in mice younger than 6 wk (32, 33). Whether this maturation also involves the mGluR system is currently unknown. Because a developmental study would be outside the focus of this study and because several groups used confocal or high-resolution STED microscopy to localize synaptic proteins in the mouse cochlea (26, 34–37), we decided to use animals of 6 wk and older and to combine confocal and STED microscopy with 3D reconstructions. A distinction between pre- and postsynaptic receptor expression was facilitated by the fact that the used antibodies recognize an epitope in the intracellular C-termini of mGluR2, mGluR4, and mGluR8b. Thus, corresponding labels appear at the intracellular sides of pre- or postsynaptic membranes, resulting in the maximal possible distance between the 2 compartments. Indeed, we could clearly separate pre- and postsynaptic marker proteins by our microscopy techniques.

MGluR2 was present at postsynaptic afferent processes of type I spiral ganglion neurons that contact the IHC ribbon synapse. There, mGluR2-specific signals partially overlapped with the postsynaptic marker protein PSD95. Whereas PSD95 was located opposite to the presynaptic ribbon, as described before (38), mGluR2-specific labeling was slightly displaced. This is in agreement with the idea that group II mGluRs are generally located outside the active zone of glutamatergic synapses (39). A presynaptic expression of group II mGluRs is widely accepted (40). A recent study analyzing group II receptors in layer III of the primate dorsolateral prefrontal cortex found mGluR2 mostly at the presynapse of glutamatergic neurons, whereas mGluR3 was expressed preferentially at the postsynaptic specializations of spines (41). The authors conclude that mGluR2 functions predominantly as autoreceptor, reducing neuronal excitation and glutamate release upon activation. However, in other CNS regions, mGluR2 was observed at postsynaptic sites (4, 42–44). Our study adds ribbon synapses of IHCs as another location within the CNS that shows a postsynaptic expression of mGluR2.

Besides cochlear hair cells, photoreceptors and bipolar cells of the retina also form ribbon synapses (45). In both tissues, mGluR2 was observed at the postsynaptic side of ribbon synapses, whereas mGluR3 was absent from this synapse type (this study, 44, 46). Unlike the cochlea, however, in the retina, mGluR2 is not present at the ribbon synapse of sensory cells (photoreceptors) but is expressed at ribbon synapses formed by second order neurons, designated as bipolar cells (44).

In contrast to mGluR2, we detected mGluR4 at the presynaptic side of IHC ribbon synapses. Again, the situation is different in the retina. Ribbon synapses of photoreceptors in the mammalian retina do not express mGluR4. Instead, this receptor is present at the postsynaptic side of ribbon synapses formed by bipolar cells, similar to mGluR2, as described in the previous paragraph (44, 47).

Ribbon synapses of photoreceptors express mGluR8 at their presynaptic site (30). There, the receptor functions as an integral part of a negative feedback loop, reducing intracellular calcium concentrations *via* a pertussis toxin sensitive G-protein, thereby regulating the glutamate concentration in the synaptic cleft (48). The immune serum used was directed against 19 aa in the C terminus of the mGluR8a isoform (residues 890–908: ETNTSSTKTTYISYSDHSI) (30). Although the N-terminal 3 aa are identical between mGluR8a and mGluR8b, the remaining sequence is specific for the mGluR8a isoform. Thus, we assume that, in this study, the distribution of mGluR8a, not mGluR8b, was actually described. We are not aware of any previous study describing in detail the localization of mGluR8b at ribbon synapses in the CNS or of mGluR8b-associated signal cascades. Recently, we identified cytosolic proteins that bind to mGluR8 types in an isoform-specific way: cannabinoid receptor interacting protein 1a (CRIP1a) regulated the endocytosis behavior of mGluR8a, but not of mGluR8b (49). Although CRIP1a was detected at the photoreceptor presynapse (50), its expression in the cochlea has not been investigated. In contrast to CRIP1a, the small ubiquitin-like modifier (SUMO) E3-ligases protein inhibitor of activated signal transducer and activator of transcription (PIAS)1 and PIAS3L interacted only with the mGluR8b isoform, but not with mGluR8a (51). Thus, we speculate that IHCs in the cochlea and photoreceptors in the retina express different mGluR8 isoforms at their ribbon synapses that permit a distinct regulation of associated signal cascades.

In recent years, it became increasingly clear that mGluRs exist as constitutive dimers (52). Dimerization of mGluRs seems to be a prerequisite for receptor activation and function (53). Besides the formation of homodimers, the authors observed the assembly of different mGluR types into heterodimeric receptor complexes. Members of group I (mGluR1 and mGluR5) can form homo- and heterodimers with themselves, but not with group II or III receptors. *Vice versa*, most of the group II and III receptors can form homo- and heterodimers with partners of these 2 groups, but not with group I receptors. Although the abovementioned receptor dimers were observed using heterologous-expressed receptors in cell lines (54), the existence of mGluR2 and mGluR4 heterodimers was shown in neurons (55). We observed mGluR2 and mGluR4 at opposite sides of the synaptic cleft, excluding a heterodimerization between these 2 receptors at the IHC ribbon synapse. On the other hand, mGluR4 and mGluR8b are both expressed presynaptically, in principle enabling the formation of heterodimers. Unfortunately, the nature of available immune sera prevented direct colocalization of mGluR4 and mGluR8b.

Certain mGluRs heterodimerize with other GPCR types, including serotonin, dopamine, and adenosine receptors (56). MGluR2 forms heterodimers with the 5-hydroxytryptamine receptor 2A (5-HT2A) serotonin receptor

using 3 aa present within the receptors transmembrane domain 4 (57, 58). However, 5-HT2A receptors are not expressed in the mouse cochlea (59). Although serotonin and serotonin synthetizing enzymes, such as tryptophan hydroxylase, were detected in afferent spiral ganglion neurons [*e.g.*, see Long *et al*. (60)], we found no evidence in the literature that these neurons express serotonin receptors at ribbon synapses of IHCs in the cochlea. In contrast to the cochlea, ribbon synapses of photoreceptors and bipolar cells in the rabbit retina do express 5-HT2A receptors (61).

For proper function, mGluRs interact with a variety of intracellular binding partners that regulate receptor trafficking, their synaptic localization, agonist sensitivity, and desensitization behavior, as well as the efficacy of G-protein coupling (62). Several proteins binding to the intracellular C-termini of mGluR2, mGluR4, and mGluR8b were identified by us and others, including the aforementioned CRIP1a and E3-ligases of the SUMOylation cascade, as well as glucocorticoid receptor interacting protein (GRIP), protein interacting with C-kinase (PICK1), Syntenin, and cytoskeleton-associated proteins such as microtubule associated protein (MAP1B) and band 4.1 proteins (49, 51, 63, 64). Of these, band 4.1 proteins were detected in IHCs of the mouse cochlea and associated with hearing deficits (65, 66). The authors localized band 4.1B, 4.1G, 4.1N, and 4.1R at stereocilia and pointed out that 4.1R interacts with myosin XV and with whirlin, 2 proteins associated with deafness. Previously, we described band 4.1 proteins as new binding partners of mGluR8 isoforms (64). Upon binding, 4.1B increased the surface expression of mGluR8b and inhibited the receptors' G-protein signaling. Although the presence of band 4.1 proteins at IHC ribbon synapses has not been analyzed so far, the above cited studies show that all 4 band 4.1 proteins are expressed in IHCs, in principle enabling an interaction with and a regulation of mGluR8b.

Our 3D reconstructions of CtBP2 fluorescent signals showed that the presynaptic ribbon is elongated into one direction, which has been previously described (24, 26). Based on electron microscopic data from IHC ribbons located in the midchochlear region, Meyer and coworkers calculated mean values for the long (228 $\pm$ 60 nm) and short (118 $\pm$ 27 nm) axis of the presynaptic ribbon. In addition, the postsynaptic density opposite to the presynaptic ribbon of IHCs was measured to be about 610 nm in length (24). Although a detailed evaluation of the dimensions of the pre- and postsynaptic structures was not of principle interest for this study, the geometry of our 3D reconstructions for CtBP2 and PSD95 are in agreement with the studies cited above.

A recent study describes functional roles of Gαi proteins at IHC ribbon synapses, influencing synaptic ribbons, synapse size, and neuronal excitability (67). The authors showed that disruption of Gαi3 signaling increased the number of calcium channel clusters and the size of the active zone. Because mGluR2, mGluR4, and mGluR8b can signal *via* Gαi proteins, these receptors might guide the activity of Gαi3 in IHCs.

Defects in hearing or vision were not reported in mice lacking mGluR2, mGluR3, mGluR4, and mGluR8 (47, 68–71). This indicates that these receptors are not primarily involved in transmitting sensory information to higher brain areas, but might be more relevant in modulating more general aspects in sensory neurons (*e.g.*, synaptic sensitivity). In doing so, the receptors could protect IHC ribbon synapses against overstimulation and resulting excitotoxic effects. Besides a genetic predisposition and inflammation, mechanical insult, such as noise trauma, can also disturb and lead to a dysfunction of the cochlear neurotransmitter systems (72, 73). Intense acoustic stimuli cause a strong presynaptic Glu release at the IHC ribbon synapse, which could overstimulate postsynaptic ionotropic glutamate receptors (24, 26). This in turn would result in an unphysiological high influx of calcium ions into postsynaptic terminals, leading to an overexcitation of spiral ganglion neurons. Furthermore, unphysiological high calcium concentrations can activate intracellular signal pathways that induce apoptotic cell death, ultimately leading to acute hearing loss (72, 74, 75). Fortunately, besides efferent innervations formed by inhibitory olivocochlear reflex loops (76), the cochlea contains inhibitory feedback loops organized locally at synapses that regulate activity and survival of sensory neurons and protect against noxious stimuli and excitotoxicity (77). The detected mGluR2, mGluR4, and mGluR8b at the IHC ribbon synapse are well suited for this task because these receptors can invert the activity of the excitatory neurotransmitter glutamate into neuronal inhibition, using intracellular signal cascades. FJ

ACKNOWLEDGMENTS

The authors thank Jean-Philippe Pin (Institut de Genomique Fonctionnelle, Montpellier, France) for providing expression constructs encoding for mGluR2 or mGluR3, Francesco Ferraguti (Innsbruck Medical University, Innsbruck, Austria) for mGluR4 antibodies, and the Optical Imaging Center Erlangen (OICE) for excellent scientific and technical support. This work was supported by the Deutsche Forschungsgemeinschaft (DFG) and the Interdisciplinary Centre for Clinical Research (IZKF) at the University Hospital of the Friedrich-Alexander-Universität Erlangen-Nürnberg. The authors declare no conflicts of interest.

AUTHOR CONTRIBUTIONS

L. Klotz performed PCR experiments, prepared and stained cochlear wholemounts, transfected and stained HEK-293 cells, stained cortical neurons and performed microscopy analysis and 3D reconstructions, as well as data evaluation and interpretation; O. Wendler prepared cochlear wholemounts and assisted with antibody staining and microscopy; R. Frischknecht prepared cortical cultures; R. Shigemoto generated and provided immune sera for mGluR8b; H. Schulze designed experiments and interpreted the microscopy data; R. Enz designed experiments, evaluated and interpreted the microscopy data and wrote the paper; and all authors read, revised and approved the manuscript.

REFERENCES

1. Fettiplace, R. (2017) Hair cell transduction, tuning, and synaptic transmission in the mammalian cochlea. *Compr. Physiol.* **7**, 1197–1227
2. Reiner, A., and Levitz, J. (2018) Glutamatergic signaling in the central nervous system: ionotropic and metabotropic receptors in concert. *Neuron* **98**, 1080–1098
3. Enz, R. (2012) Metabotropic glutamate receptors and interacting proteins: evolving drug targets. *Curr. Drug Targets* **13**, 145–156
4. Tamaru, Y., Nomura, S., Mizuno, N., and Shigemoto, R. (2001) Distribution of metabotropic glutamate receptor mGluR3 in the mouse CNS: differential location relative to pre- and postsynaptic sites. *Neuroscience* **106**, 481–503
5. Martemyanov, K. A. (2014) G protein signaling in the retina and beyond: the Cogan lecture. *Invest. Ophthalmol. Vis. Sci.* **55**, 8201–8207
6. Goutman, J. D., Elgoyhen, A. B., and Gómez-Casati, M. E. (2015) Cochlear hair cells: the sound-sensing machines. *FEBS Lett.* **589**, 3354–3361
7. Takago, H., and Oshima-Takago, T. (2018) Pre- and postsynaptic ionotropic glutamate receptors in the auditory system of mammals. *Hear. Res.* **362**, 1–13
8. Lu, Y. (2014) Metabotropic glutamate receptors in auditory processing. *Neuroscience* **274**, 429–445
9. Doleviczényi, Z., Halmos, G., Répássy, G., Vizi, E. S., Zelles, T., and Lendvai, B. (2005) Cochlear dopamine release is modulated by group II metabotropic glutamate receptors via GABAergic neurotransmission. *Neurosci. Lett.* **385**, 93–98
10. Van Laer, L., Huyghe, J. R., Hannula, S., Van Eyken, E., Stephan, D. A., Mäki-Torkko, E., Aikio, P., Fransen, E., Lysholm-Bernacchi, A., Sorri, M., Huentelman, M. J., and Van Camp, G. (2010) A genome-wide association study for age-related hearing impairment in the Saami. *Eur. J. Hum. Genet.* **18**, 685–693
11. Yu, P., Jiao, J., Chen, G., Zhou, W., Zhang, H., Wu, H., Li, Y., Gu, G., Zheng, Y., Yu, Y., and Yu, S. (2018) Effect of GRM7 polymorphisms on the development of noise-induced hearing loss in Chinese Han workers: a nested case-control study. *BMC Med. Genet.* **19**, 4
12. Friedman, R. A., Van Laer, L., Huentelman, M. J., Sheth, S. S., Van Eyken, E., Corneveaux, J. J., Tembe, W. D., Halperin, R. F., Thorburn, A. Q., Thys, S., Bonneux, S., Fransen, E., Huyghe, J., Pyykkö, I., Cremers, C. W., Kremer, H., Dhooge, I., Stephens, D., Orzan, E., Pfister, M., Bille, M., Parving, A., Sorri, M., Van de Heyning, P. H., Makmura, L., Ohmen, J. D., Linthicum, F. H., Jr., Fayad, J. N., Pearson, J. V., Craig, D. W., Stephan, D. A., and Van Camp, G. (2009) GRM7 variants confer susceptibility to age-related hearing impairment. *Hum. Mol. Genet.* **18**, 785–796
13. Newman, D. L., Fisher, L. M., Ohmen, J., Parody, R., Fong, C. T., Frisina, S. T., Mapes, F., Eddins, D. A., Robert Frisina, D., Frisina, R. D., and Friedman, R. A. (2012) GRM7 variants associated with age-related hearing loss based on auditory perception. *Hear. Res.* **294**, 125–132
14. Girotto, G., Vuckovic, D., Buniello, A., Lorente-Cánovas, B., Lewis, M., Gasparini, P., and Steel, K. P. (2014) Expression and replication studies to identify new candidate genes involved in normal hearing function. *PLoS One* **9**, e85352; erratum: e91446
15. Wan, G., and Corfas, G. (2015) No longer falling on deaf ears: mechanisms of degeneration and regeneration of cochlear ribbon synapses. *Hear. Res.* **329**, 1–10
16. Liberman, M. C., and Kujawa, S. G. (2017) Cochlear synaptopathy in acquired sensorineural hearing loss: manifestations and mechanisms. *Hear. Res.* **349**, 138–147
17. Valenzuela, J. C., Heise, C., Franken, G., Singh, J., Schweitzer, B., Seidenbecher, C. I., and Frischknecht, R. (2014) Hyaluronan-based extracellular matrix under conditions of homeostatic plasticity. *Philos. Trans. R. Soc. Lond. B Biol. Sci.* **369**, 20130606
18. Corti, C., Aldegheri, L., Somogyi, P., and Ferraguti, F. (2002) Distribution and synaptic localisation of the metabotropic glutamate receptor 4 (mGluR4) in the rodent CNS. *Neuroscience* **110**, 403–420
19. Ferraguti, F., Klausberger, T., Cobden, P., Baude, A., Roberts, J. D., Szucs, P., Kinoshita, A., Shigemoto, R., Somogyi, P., and Dalezios, Y. (2005) Metabotropic glutamate receptor 8-expressing nerve terminals target subsets of GABAergic neurons in the hippocampus. *J. Neurosci.* **25**, 10520–10536
20. Seebahn, A., Rose, M., and Enz, R. (2008) RanBPM is expressed in synaptic layers of the mammalian retina and binds to metabotropic glutamate receptors. *FEBS Lett.* **582**, 2453–2457
21. Brandstätter, J. H., Koulen, P., Kuhn, R., van der Putten, H., and Wässle, H. (1996) Compartmental localization of a metabotropic glutamate receptor (mGluR7): two different active sites at a retinal synapse. *J. Neurosci.* **16**, 4749–4756
22. Schmitz, F., Königstorfer, A., and Südhof, T. C. (2000) RIBEYE, a component of synaptic ribbons: a protein's journey through evolution provides insight into synaptic ribbon function. *Neuron* **28**, 857–872
23. Martinez-Monedero, R., Liu, C., Weisz, C., Vyas, P., Fuchs, P. A., and Glowatzki, E. (2016) GluA2-containing AMPA receptors distinguish ribbon-associated from ribbonless afferent contacts on rat cochlear hair cells. *eNeuro* **3**, ENEURO.0078-16.2016
24. Wong, A. B., Rutherford, M. A., Gabrielaitis, M., Pangrsic, T., Göttfert, F., Frank, T., Michanski, S., Hell, S., Wolf, F., Wichmann, C., and Moser, T. (2014) Developmental refinement of hair cell synapses tightens the coupling of Ca2+ influx to exocytosis. *EMBO J.* **33**, 247–264
25. Khimich, D., Nouvian, R., Pujol, R., Tom Dieck, S., Egner, A., Gundelfinger, E. D., and Moser, T. (2005) Hair cell synaptic ribbons are essential for synchronous auditory signalling. *Nature* **434**, 889–894
26. Meyer, A. C., Frank, T., Khimich, D., Hoch, G., Riedel, D., Chapochnikov, N. M., Yarin, Y. M., Harke, B., Hell, S. W., Egner, A., and Moser, T. (2009) Tuning of synapse number, structure and function in the cochlea. *Nat. Neurosci.* **12**, 444–453
27. Vogl, C., Cooper, B. H., Neef, J., Wojcik, S. M., Reim, K., Reisinger, E., Brose, N., Rhee, J. S., Moser, T., and Wichmann, C. (2015) Unconventional molecular regulation of synaptic vesicle replenishment in cochlear inner hair cells. *J. Cell Sci.* **128**, 638–644
28. Koga, K., Iwahori, Y., Ozaki, S., and Ohta, H. (2010) Regulation of spontaneous Ca(2+) spikes by metabotropic glutamate receptors in primary cultures of rat cortical neurons. *J. Neurosci. Res.* **88**, 2252–2262
29. Suzuki, S., Koshimizu, H., Adachi, N., Matsuoka, H., Fushimi, S., Ono, J., Ohta, K. I., and Miki, T. (2017) Functional interaction between BDNF and mGluR II *in vitro*: BDNF down-regulated mGluR II gene expression and an mGluR II agonist enhanced BDNF-induced BDNF gene expression in rat cerebral cortical neurons. *Peptides* **89**, 42–49
30. Koulen, P., Kuhn, R., Wässle, H., and Brandstätter, J. H. (1999) Modulation of the intracellular calcium concentration in photoreceptor terminals by a presynaptic metabotropic glutamate receptor. *Proc. Natl. Acad. Sci. USA* **96**, 9909–9914
31. Brandstätter, J. H., Koulen, P., and Wässle, H. (1998) Diversity of glutamate receptors in the mammalian retina. *Vision Res.* **38**, 1385–1397
32. Frank, M. M., and Goodrich, L. V. (2018) Talking back: development of the olivocochlear efferent system. *Wiley Interdiscip. Rev. Dev. Biol.* **7**, e324
33. Roux, I., Wu, J. S., McIntosh, J. M., and Glowatzki, E. (2016) Assessment of the expression and role of the α1-nAChR subunit in efferent cholinergic function during the development of the mammalian cochlea. *J. Neurophysiol.* **116**, 479–492
34. Brandt, A., Khimich, D., and Moser, T. (2005) Few CaV1.3 channels regulate the exocytosis of a synaptic vesicle at the hair cell ribbon synapse. *J. Neurosci.* **25**, 11577–11585
35. Neef, J., Urban, N. T., Ohn, T. L., Frank, T., Jean, P., Hell, S. W., Willig, K. I., and Moser, T. (2018) Quantitative optical nanophysiology of Ca^{2+} signaling at inner hair cell active zones. *Nat. Commun.* **9**, 290
36. Jung, S., Oshima-Takago, T., Chakrabarti, R., Wong, A. B., Jing, Z., Yamanbaeva, G., Picher, M. M., Wojcik, S. M., Göttfert, F., Predoehl, F., Michel, K., Hell, S. W., Schoch, S., Strenzke, N., Wichmann, C., and Moser, T. (2015) Rab3-interacting molecules 2α and 2β promote the abundance of voltage-gated CaV1.3 Ca2+ channels at hair cell active zones. *Proc. Natl. Acad. Sci. USA* **112**, E3141–E3149
37. Fujikawa, T., Petralia, R. S., Fitzgerald, T. S., Wang, Y. X., Millis, B., Morgado-Díaz, J. A., Kitamura, K., and Kachar, B. (2014) Localization of kainate receptors in inner and outer hair cell synapses. *Hear. Res.* **314**, 20–32
38. Tong, M., Brugeaud, A., and Edge, A. S. (2013) Regenerated synapses between postnatal hair cells and auditory neurons. *J. Assoc. Res. Otolaryngol.* **14**, 321–329
39. Ferraguti, F., and Shigemoto, R. (2006) Metabotropic glutamate receptors. *Cell Tissue Res.* **326**, 483–504
40. Johnson, K. A., and Lovinger, D. M. (2016) Presynaptic G protein-coupled receptors: gatekeepers of addiction? *Front. Cell. Neurosci.* **10**, 264
41. Jin, L. E., Wang, M., Galvin, V. C., Lightbourne, T. C., Conn, P. J., Arnsten, A. F. T., and Paspalas, C. D. (2018) mGluR2 versus mGluR3 metabotropic glutamate receptors in primate dorsolateral prefrontal cortex: postsynaptic mGluR3 strengthen working memory networks. *Cereb. Cortex* **28**, 974–987

42. Petralia, R. S., Wang, Y. X., Zhao, H. M., and Wenthold, R. J. (1996) Ionotropic and metabotropic glutamate receptors show unique postsynaptic, presynaptic, and glial localizations in the dorsal cochlear nucleus. *J. Comp. Neurol.* **372**, 356–383
43. Petralia, R. S., Wang, Y. X., Niedzielski, A. S., and Wenthold, R. J. (1996) The metabotropic glutamate receptors, mGluR2 and mGluR3, show unique postsynaptic, presynaptic and glial localizations. *Neuroscience* **71**, 949–976
44. Koulen, P., Malitschek, B., Kuhn, R., Wässle, H., and Brandstätter, J. H. (1996) Group II and group III metabotropic glutamate receptors in the rat retina: distributions and developmental expression patterns. *Eur. J. Neurosci.* **8**, 2177–2187
45. Tom Dieck, S., and Brandstätter, J. H. (2006) Ribbon synapses of the retina. *Cell Tissue Res.* **326**, 339–346
46. Hartveit, E., Brandstätter, J. H., Enz, R., and Wässle, H. (1995) Expression of the mRNA of seven metabotropic glutamate receptors (mGluR1 to 7) in the rat retina. An *in situ* hybridization study on tissue sections and isolated cells. *Eur. J. Neurosci.* **7**, 1472–1483
47. Quraishi, S., Gayet, J., Morgans, C. W., and Duvoisin, R. M. (2007) Distribution of group-III metabotropic glutamate receptors in the retina. *J. Comp. Neurol.* **501**, 931–943
48. Koulen, P., Liu, J., Nixon, E., and Madry, C. (2005) Interaction between mGluR8 and calcium channels in photoreceptors is sensitive to pertussis toxin and occurs via G protein betagamma subunit signaling. *Invest. Ophthalmol. Vis. Sci.* **46**, 287–291
49. Mascia, F., Klotz, L., Lerch, J., Ahmed, M. H., Zhang, Y., and Enz, R. (2017) CRIP1a inhibits endocytosis of G-protein coupled receptors activated by endocannabinoids and glutamate by a common molecular mechanism. *J. Neurochem.* **141**, 577–591
50. Hu, S. S., Arnold, A., Hutchens, J. M., Radicke, J., Cravatt, B. F., Wager-Miller, J., Mackie, K., and Straiker, A. (2010) Architecture of cannabinoid signaling in mouse retina. *J. Comp. Neurol.* **518**, 3848–3866
51. Dütting, E., Schröder-Kress, N., Sticht, H., and Enz, R. (2011) SUMO E3 ligases are expressed in the retina and regulate SUMOylation of the metabotropic glutamate receptor 8b. *Biochem. J.* **435**, 365–371
52. Doumazane, E., Scholler, P., Zwier, J. M., Trinquet, E., Rondard, P., and Pin, J. P. (2011) A new approach to analyze cell surface protein complexes reveals specific heterodimeric metabotropic glutamate receptors. *FASEB J.* **25**, 66–77
53. Møller, T. C., Moreno-Delgado, D., Pin, J. P., and Kniazeff, J. (2017) Class C G protein-coupled receptors: reviving old couples with new partners. *Biophys. Rep.* **3**, 57–63
54. Yin, S., Noetzel, M. J., Johnson, K. A., Zamorano, R., Jalan-Sakrikar, N., Gregory, K. J., Conn, P. J., and Niswender, C. M. (2014) Selective actions of novel allosteric modulators reveal functional heteromers of metabotropic glutamate receptors in the CNS. *J. Neurosci.* **34**, 79–94
55. Moreno Delgado, D., Møller, T. C., Ster, J., Giraldo, J., Maurel, D., Rovira, X., Scholler, P., Zwier, J. M., Perroy, J., Durroux, T., Trinquet, E., Prezeau, L., Rondard, P., and Pin, J. P. (2017) Pharmacological evidence for a metabotropic glutamate receptor heterodimer in neuronal cells. *eLife* **6**, e25233
56. Pin, J. P., and Bettler, B. (2016) Organization and functions of mGlu and $GABA_B$ receptor complexes. *Nature* **540**, 60–68
57. González-Maeso, J., Ang, R. L., Yuen, T., Chan, P., Weisstaub, N. V., López-Giménez, J. F., Zhou, M., Okawa, Y., Callado, L. F., Milligan, G., Gingrich, J. A., Filizola, M., Meana, J. J., and Sealfon, S. C. (2008) Identification of a serotonin/glutamate receptor complex implicated in psychosis. *Nature* **452**, 93–97
58. Moreno, J. L., Muguruza, C., Umali, A., Mortillo, S., Holloway, T., Pilar-Cuéllar, F., Mocci, G., Seto, J., Callado, L. F., Neve, R. L., Milligan, G., Sealfon, S. C., López-Giménez, J. F., Meana, J. J., Benson, D. L., and González-Maeso, J. (2012) Identification of three residues essential for 5-hydroxytryptamine 2A-metabotropic glutamate 2 (5-HT2A·mGlu2) receptor heteromerization and its psychoactive behavioral function. *J. Biol. Chem.* **287**, 44301–44319
59. Oh, C. K., Drescher, M. J., Hatfield, J. S., and Drescher, D. G. (1999) Selective expression of serotonin receptor transcripts in the mammalian cochlea and its subdivisions. *Brain Res. Mol. Brain Res.* **70**, 135–140
60. Long, L., Xie, X., and Tang, Y. (2018) Distribution of tryptophan hydroxylase immunoreactivity in the spiral Ganglion neurons of mouse cochlea. *Indian J. Otolaryngol. Head Neck Surg.* **70**, 425–427
61. Pootanakit, K., Prior, K. J., Hunter, D. D., and Brunken, W. J. (1999) 5-HT2a receptors in the rabbit retina: potential presynaptic modulators. *Vis. Neurosci.* **16**, 221–230
62. Enz, R. (2012) Structure of metabotropic glutamate receptor C-terminal domains in contact with interacting proteins. *Front. Mol. Neurosci.* **5**, 52
63. Enz, R. (2007) The trick of the tail: protein-protein interactions of metabotropic glutamate receptors. *BioEssays* **29**, 60–73
64. Rose, M., Dütting, E., and Enz, R. (2008) Band 4.1 proteins are expressed in the retina and interact with both isoforms of the metabotropic glutamate receptor type 8. *J. Neurochem.* **105**, 2375–2387
65. Mburu, P., Kikkawa, Y., Townsend, S., Romero, R., Yonekawa, H., and Brown, S. D. (2006) Whirlin complexes with p55 at the stereocilia tip during hair cell development. *Proc. Natl. Acad. Sci. USA* **103**, 10973–10978
66. Okumura, K., Mochizuki, E., Yokohama, M., Yamakawa, H., Shitara, H., Mburu, P., Yonekawa, H., Brown, S. D., and Kikkawa, Y. (2010) Protein 4.1 expression in the developing hair cells of the mouse inner ear. *Brain Res.* **1307**, 53–62
67. Jean, P., Özçete, Ö. D., Tarchini, B., and Moser, T. (2019) Intrinsic planar polarity mechanisms influence the position-dependent regulation of synapse properties in inner hair cells. *Proc. Natl. Acad. Sci. USA* **116**, 9084–9093
68. Corti, C., Battaglia, G., Molinaro, G., Riozzi, B., Pittaluga, A., Corsi, M., Mugnaini, M., Nicoletti, F., and Bruno, V. (2007) The use of knock-out mice unravels distinct roles for mGlu2 and mGlu3 metabotropic glutamate receptors in mechanisms of neurodegeneration/neuroprotection. *J. Neurosci.* **27**, 8297–8308
69. Linden, A. M., Johnson, B. G., Trokovic, N., Korpi, E. R., and Schoepp, D. D. (2009) Use of MGLUR2 and MGLUR3 knockout mice to explore *in vivo* receptor specificity of the MGLUR2/3 selective antagonist LY341495. *Neuropharmacology* **57**, 172–182
70. Pekhletski, R., Gerlai, R., Overstreet, L. S., Huang, X. P., Agopyan, N., Slater, N. T., Abramow-Newerly, W., Roder, J. C., and Hampson, D. R. (1996) Impaired cerebellar synaptic plasticity and motor performance in mice lacking the mGluR4 subtype of metabotropic glutamate receptor. *J. Neurosci.* **16**, 6364–6373
71. Duvoisin, R. M., Zhang, C., Pfankuch, T. F., O'Connor, H., Gayet-Primo, J., Quraishi, S., and Raber, J. (2005) Increased measures of anxiety and weight gain in mice lacking the group III metabotropic glutamate receptor mGluR8. *Eur. J. Neurosci.* **22**, 425–436
72. Nouvian, R., Eybalin, M., and Puel, J. L. (2015) Cochlear efferents in developing adult and pathological conditions. *Cell Tissue Res.* **361**, 301–309
73. Ruel, J., Wang, J., Rebillard, G., Eybalin, M., Lloyd, R., Pujol, R., and Puel, J. L. (2007) Physiology, pharmacology and plasticity at the inner hair cell synaptic complex. *Hear. Res.* **227**, 19–27
74. Liberman, M. C. (2016) Noise-induced hearing loss: permanent versus temporary threshold shifts and the effects of hair cell versus neuronal degeneration. *Adv. Exp. Med. Biol.* **875**, 1–7
75. Pujol, R., and Puel, J. L. (1999) Excitotoxicity, synaptic repair, and functional recovery in the mammalian cochlea: a review of recent findings. *Ann. N. Y. Acad. Sci.* **884**, 249–254
76. Terreros, G., and Delano, P. H. (2015) Corticofugal modulation of peripheral auditory responses. *Front. Syst. Neurosci.* **9**, 134
77. Masilamoni, G. J., and Smith, Y. (2018) Metabotropic glutamate receptors: targets for neuroprotective therapies in Parkinson disease. *Curr. Opin. Pharmacol.* **38**, 72–80

Received for publication June 25, 2019.
Accepted for publication September 3, 2019.